

Lawrence Berkeley National Laboratory

LBL Publications

Title

Microbial contribution to post-fire tundra ecosystem recovery over the 21st century

Permalink

<https://escholarship.org/uc/item/8888r6jw>

Journal

Communications Earth & Environment, 3(1)

ISSN

2662-4435

Authors

Bouskill, Nicholas J

Mekonnen, Zelalem

Zhu, Qing

et al.

Publication Date




2022

DOI

10.1038/s43247-022-00356-2

Peer reviewed

Microbial contribution to post-fire tundra ecosystem recovery over the 21st century

Nicholas J. Bouskill ¹✉, Zelalem Mekonnen ¹, Qing Zhu ^{1,2}, Robert Grant³ & William J. Riley¹

Tundra ecosystems have experienced an increased frequency of fire, and this trend is predicted to continue throughout the 21st Century. Post-fire recovery is underpinned by complex interactions between microbial functional groups that drive nutrient cycling. Here we use a mechanistic model to demonstrate an acceleration of the nitrogen cycle post-fire driven by changes in niche space and microbial competitive dynamics. We show that over the first 5-years post-fire, fast-growing bacterial heterotrophs colonize regions of the soil previously occupied by slower-growing saprotrophic fungi. The bacterial heterotrophs mineralize organic matter, releasing nutrients into the soil. This pathway outweighs new sources of nitrogen and facilitates the recovery of plant productivity. We broadly show here that while consideration of distinct microbial metabolisms related to carbon and nutrient cycling remains rare in terrestrial ecosystem models, they are important when considering the rate of ecosystem recovery post-disturbance and the feedback to soil nutrient cycles on centennial timescales.

¹Climate and Ecosystem Sciences Division, Lawrence Berkeley National Laboratory, Berkeley, CA 94720, USA. ²Berkeley Institute of Data Science, University of California, Berkeley, CA 94720, USA. ³Department of Renewable Resources, University of Alberta, Edmonton, AB, Canada. ✉email: njbouskill@lbl.gov

The vast organic matter stocks in arctic permafrost soils (~1000 PgC in the top 3 m^{1–3}) have the potential to contribute positively to rising atmospheric carbon dioxide concentrations and the carbon-climate feedback. Air temperatures in Arctic regions are currently warming at twice the global average rate (0.6 °C per decade)⁴, which can stimulate microbial decomposition and accelerate the turnover of the soil organic matter (SOM) stocks to greenhouse gases (CO₂, CH₄, and N₂O). However, rising air temperatures also drive increased drought⁵, higher vapor pressure deficits^{6,7}, and lightning⁸, contributing to an increased frequency and intensity of tundra fires^{9–11}.

Fires represent a profound disturbance to high-latitude ecosystems. The aftermath of a fire alters the surface energy balance¹²; alters soil hydrodynamics^{13,14}; reduces soil carbon stocks, including ancient carbon previously sequestered within permafrost¹⁵; increases soil nutrient losses¹⁶; and causes shifts in plant and microbial community composition^{17,18}. Depending on fire severity and depth of the burn, fire ramifications on ecosystem thermal, chemical, and biological features can be apparent for several decades post-fire^{12,19}. However, how abrupt disturbances, such as fire, shape ecosystem responses to climate change, including to soil carbon stocks, remains uncertain.

Broad impacts of fire on tundra plant communities have been reasonably well characterized^{17,20–22}, and differences in recovery have been demonstrated for vascular plants and cryptogams (e.g., moss and lichen)¹⁷. Shrubs and graminoids regenerate quite rapidly from soil seed banks, and increase in abundance post-fire^{21,23,24}. However, the timescale for recovery differs between the two plant types, with rapid recovery shown for graminoids¹⁷, relative to shrubs, which can take more than a decade to reestablish²². However, fires have also been shown to elevate shrub expansion relative to prefire conditions, hastening transitions that would otherwise take decades²². Cryptogams, by contrast, have no fire survival strategies, and tend to be decimated by fire²⁵. Their recovery is often very slow due to a need for recolonization post-fire via airborne spores originating from unburned regions.

Belowground, fire acts as a direct disturbance to microbial communities through heat-induced mortality and shifting community composition in the upper soil layers^{26–28}. Fire also acts on the microbial community indirectly by changing nutrient availability²⁹, and the quality and quantity of carbon sources³⁰, shaping the metabolic diversity of belowground communities¹⁸. Microbes also differ in their sensitivity to fire and recovery post-fire, whereby bacteria recover more quickly relative to fungi^{28,31,32}. However, Hewitt et al.³³ noted that, while increasingly severe fire reduces the relative abundance of fungal taxa, mycorrhizal fungi can become more resilient to fire through the resprouting life-history of tundra shrubs maintaining an inoculum source post-fire³³. Recovery of microbial communities post-fire is critical to organic matter decomposition and nutrient cycling and availability, which drives vegetation recovery. However, the sequence of events that facilitate a reversion to ecosystem steady-state post-fire, including the links between microbial and plant communities, remain difficult to demonstrate empirically. In addition to the effects of fire, shrub expansion under a warming climate^{34,35} can change the composition of belowground communities³⁶. Shrubs tend to produce litter with higher carbon to nitrogen ratios, encouraging the growth of fungi with lower nitrogen requirements relative to bacteria³⁷. This pattern is important as the role fungi play in soil carbon cycling can be distinct from that of bacteria, partly because fungi produce chemically recalcitrant biomass, which slows rates of decomposition³⁸. Therefore, climate–fire interactions that shape vegetation and microbial community composition will feedback on the tundra carbon cycle^{39,40}.

Here we apply observations and a well-tested mechanistic model, *ecosys*, to address the question of how disturbance from a tundra fire interacts with longer-term climate perturbations (i.e., warming, increasing CO₂ concentrations, and elevated precipitation). The *ecosys* model simulates the interdependent physical, hydrological, and biological processes that govern ecosystem responses to perturbation. The model, which includes mechanistic representations of carbon, water, nitrogen, and phosphorus dynamics in plants and soils, has been successfully applied in dozens of sites around the world, with many studies focusing on high-latitude ecosystems^{41–45}. Further information on model structure and performance in tundra ecosystems is available in the materials and methods section below. We focus our model experiments on one of the largest tundra fires on record, the 2007 Anaktuvuk River Fire, Alaska, which was caused by lightning and exacerbated by record high summer temperatures and record low summer precipitation^{23,46,47}. The present study simulates the ecosystem responses to, and recovery from, that fire. We initially parameterize and benchmark the model using the available data built up around this well-studied fire^{15,17,23,47,48}. Once benchmarked, we conduct modeling experiments to address three main questions: (1) What are the long-term ramifications of fire disturbance against the backdrop of ongoing climate change across the 21st century? (2) What role does the belowground microbial community play in enabling the recovery of the aboveground plant community? (3) How does recovery post-wildfire differ between an early 21st century graminoid dominated ecosystem, and a late century shrub-dominated ecosystem with high shrub abundance?

Results

We next describe: (1) *ecosys* model testing at the Anaktuvuk River site; (2) 21st century carbon and nitrogen cycling in the absence of fire; (3) fire effects on 21st century carbon cycling; (4) fire effects on 21st century soil moisture and temperature; and (5) fire effects on 21st century belowground microbial community structure and nutrient cycling.

Model testing at the Anaktuvuk River site. We evaluated the model against data collected from the severe 2007 Anaktuvuk River fire. Data was collected on plant community metrics¹⁷, soil carbon¹⁵, and site physical factors²³. Figure 1 shows agreement between measured and simulated values (normalized Root Mean Square Error (RMSE) = 0.037). The model replicated the annual net primary productivity (NPP) of the ecosystem before (~200 ± 40 g m⁻² yr⁻¹) and 4 years after (~160 ± 10 g m⁻² yr⁻¹) the fire. Further, the model performed well in replicating the NPP of individual plant functional types (PFTs) (Figs. 1, S2a), with graminoids making up ~60% of the vegetation (observation: ~125 gC m⁻² yr⁻¹; simulation: 120 ± 40 gC m⁻² yr⁻¹) prior to fire, and shrubs accounting for most of the remainder (observation: 75 gC m⁻² yr⁻¹; simulation: 75 ± 20 gC m⁻² yr⁻¹; Supplementary Fig. 2). Nonvascular plants were present but represented a small (~3 %) fraction of NPP in observations and the simulation. A more recent analysis of PFT composition at this site has demonstrated a shift in the community a decade post-fire. While graminoids are still a major part of the community, deciduous shrubs, rather than evergreens, account for a greater proportion of the shrubs.

prefire total (to 0.2 m depth) soil carbon content reported for this site ranged from 2842 gC m⁻² to nearly 20 kgC m⁻² (depending on the depth of the soil organic layer, which ranged from 12.3 to 43.3 cm). The simulated prefire 0–20 cm depth soil carbon content is 6320 ± 355 gC m⁻², which is consistent with a reported value of 7682 ± 766 gC m⁻² from 0 to 21.5 cm depth¹⁵.

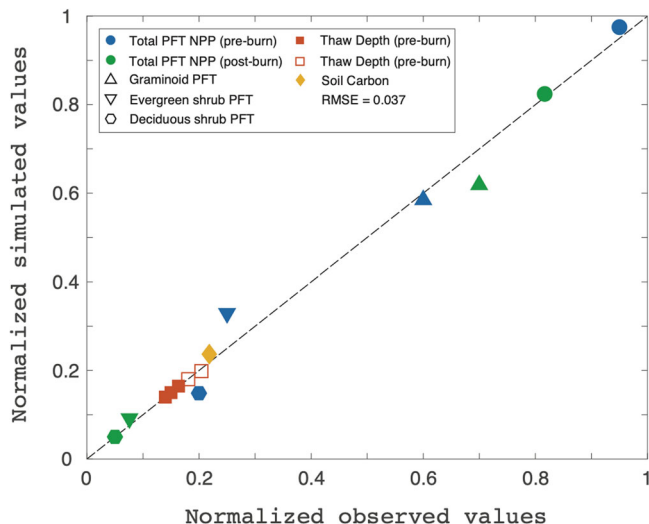


Fig. 1 Model benchmarks against the observational data taken before and after the 2007 Anaktuvik severe fire. The benchmarks include net primary productivity (total and PFT specific), active layer depth pre- and post-fire, and soil carbon stocks. The NPP data are separately reported for the unburned ecosystem (blue symbols) and post-fire plots (green symbols). For ease of visualization, the figure provides comparisons between the normalized data; individual benchmark comparisons, including the time of data collection, are provided in the supplemental material (Supplementary Fig. 2).

Table 1 RCP8.5 driven changes in atmospheric variables.

	Max. Temp. (°C)	Min. Temp. (°C)	Precipitation	C _a
Winter (DJF)	10.97	12.80	1.34	2.37
Spring (MAM)	7.08	8.28	1.52	2.37
Summer (JJA)	4.53	4.84	1.28	2.37
Autumn (SON)	7.25	8.30	1.34	2.37

The table provides the average seasonal increases between years 2071–2100 relative to current values (1981–2010). Shown here are the increases in maximum and minimum temperatures, precipitation, and atmospheric CO₂ concentration (C_a) under the RCP8.5 emission scenario downscaled and averaged across 15 CMIP5 models for the Anaktuvik River, Alaska gridcell.

Total modeled soil carbon concentration from 0 to 1 m depth was 42.3 kgC m⁻². Finally, thaw depth pre- and post-fire was accurately modeled compared to the observations (Figs. 1, S2b).

These results, alongside previously described evaluations of the model applied to high-latitude ecosystems with⁴⁰ and without fire^{41,42,49,50}, demonstrate that *ecosys* provides a reasonable representation of tundra ecosystems, and can be extended to our 21st century model experiments.

21st century carbon and nitrogen cycling in the absence of fire.

We first evaluated the site responses under the baseline RCP8.5 scenario (Table 1), which did not have fire. Over the 21st century the site NPP more than doubled, from ~200 gC m⁻² yr⁻¹ to ~530 gC m⁻² yr⁻¹ (Fig. 2a), and despite a large increase in ecosystem respiration (heterotrophic + autotrophic), the soil became a stronger net sink for atmospheric carbon (Fig. 2b). Increased shrub abundance and growth, particularly of evergreen shrubs, were simulated throughout the 21st century and accounted for much of the elevated NPP by 2100.

Consistent with the stronger ecosystem sink by 2100, soil carbon slightly increased over time, accumulating (0.67 kgC m⁻²;

1.5%) by 2100. Methane emissions increase over the 21st Century but remained low, while nitrous oxide (N₂O) production generally becomes more variable over time (Fig. 2b), alongside an increase in soil nitrogen concentrations, yet does not show a clear trajectory of increasing emissions. The active layer depth increases slowly to 50 cm at year 2060 before deepening more rapidly to ~90 cm by the end of the century. Corresponding increases in soil moisture were simulated, with a slow increase in the shallower soil (surface to ~0.3 m depth), and a rapid increase at ~0.5 m in line with a drop in the ALD (Fig. 2c). Toward the end of the century, as the ALD deepens beyond 1 m, soil moisture at depth also increases rapidly. Soil temperature demonstrates a similar response, increasing over time from an annual average of -2 °C within surface soils, to a temperature of +3 °C by the end of the century (Fig. 2c).

Increasing thaw depth, soil carbon, temperature, and moisture provided additional niches for growth and activity of microorganisms. Over the 21st Century under the RCP8.5 scenario, microbial biomass increased (Fig. 2d), notably within surface soils, but also at depth (>0.5 m) concurrent with increasing thaw depth. Within the 0–0.2 m depth interval, much of the simulated increases were attributable to increasing fungal biomass, concordant with increasing shrub biomass and a lower litter quality (C:N ratio), that resulted in a higher fungal:bacterial biomass ratio over time (Fig. 2e).

The transfer entropy approach adopted here identifies the most important factors leading to the annual increases in simulated ecosystem NPP. Notably, nutrient cycling and plant assimilation are critical to plant NPP throughout the century (Supplementary Fig. 3a/b). Additional factors contributing to increased NPP include increased snowpack depth, soil moisture, and soil temperature. These factors all contribute to increased root and mycorrhizal growth and microbial mineralization responsible for nutrient release.

Fire effects on 21st century carbon cycling.

We next evaluated how pulsed perturbation (fires of various severities) impact this tundra ecosystem under a continuing RCP8.5 press perturbation (climate change). The modeled depth of burn and extent of organic matter combustion associated with fires of different severities are determined from previously published syntheses⁵¹ (and provide in Table 2).

These fire perturbations were applied during two timeframes: (i) early in the century (during 2007) under a graminoid-dominated ecosystem, and (ii) later in the century (in 2080) when woody shrubs dominate ecosystem biomass. Fire prescribed in both 2007 and 2080 significantly reduced soil carbon stocks through combustion by a maximum of ~2400 gC m⁻² under the severe fire conditions, and less under moderate (1400 gC m⁻²) and mild (550 gC m⁻²) severity fires (Fig. 3). The severe fire modeled values are consistent with observed values of net carbon loss of 2016 gC m⁻² measured a year following the actual Anaktuvik severe 2007 fire¹⁵. The recovery of modeled soil carbon stocks in the 20 years post-fire showed clear differences between fires initiated in 2007 and in 2080, and between fires of different severity. Following a fire of mild-severity ignited in 2080 soil carbon stocks equilibrated to prefire conditions after 8 years, and thereafter exceeded initial conditions (Fig. 3b). By contrast, soil carbon stocks burned in all the other fire simulations did not return to prefire conditions 20 years post fire (Fig. 3a). However, soil carbon stocks following late-century moderate and severe fires rebounded to their new quasi-steady condition more rapidly than those following early century fires.

Net primary productivity decreased more strongly following late- than early-century fires (Fig. 4a). Notably, the post-fire

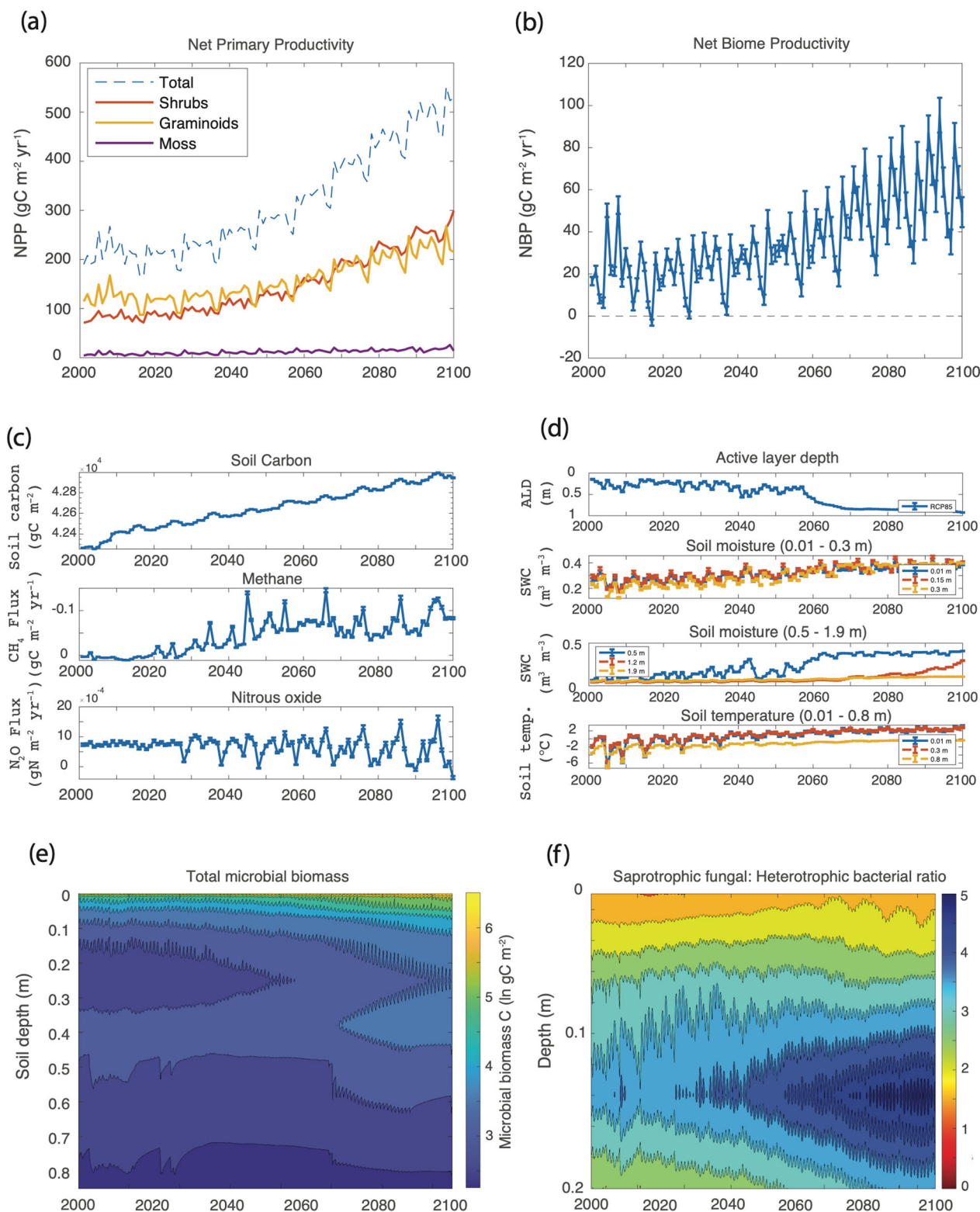


Fig. 2 Ecosystem trajectories under the baseline RCP8.5-no_fire scenario for the period 2000–2100. The panels show **a** changes in net primary productivity (gC m^{-2}) for the total plant ecosystem and by plant functional type, **b** net biome productivity ($\text{gC m}^{-2} \text{yr}^{-1}$), **c** soil carbon stocks down to 1 m (gC m^{-2}) and surface methane ($\text{gC m}^{-2} \text{yr}^{-1}$) and nitrous oxide ($\text{gN m}^{-2} \text{yr}^{-1}$) fluxes, **d** physical and hydrological responses. The panels depict (from top to bottom), the active layer depth (m), soil moisture in surface soils at 0.01–0.3 m and deeper down (0.5–1.9 m) depths ($\text{m}^3 \text{m}^{-3}$), and soil temperature ($^{\circ}\text{C}$) at three soil depths (0.01, 0.3 and 0.8 m), **e** total microbial biomass down to 0.85 m depth (units of $\ln \text{gC m}^{-2}$), and **f** the biomass ratio of saprotrophic fungi to heterotrophic bacteria (aerobic + facultative heterotrophs) in the top 20 cm of soil.

Table 2 Perturbation scenarios over the 21st century.

Scenario name	Perturbation	Depth of burn	% OM combustion	Year of fire ^a
RCP8.5-no_fire	CF ^b	N/A	N/A	N/A
Mild 1	CF + Fire	5 cm	25%	2007
Mild 2	CF + Fire	5 cm	25%	2080
Moderate 1	CF + Fire	11 cm	50%	2007
Moderate 2	CF + Fire	11 cm	50%	2080
Severe 1	CF + Fire	16 cm	85%	2007
Severe 2	CF + Fire	16 cm	85%	2080

^aAll simulations are run between 1900 and 2100, and the fire is initiated in the first year of each focal length period. The analyses below may represent a focal length of 20-years post-fire, or out to 2100.

^bCF: Climate Forcing; represents the predicted changes in air temperature, radiative forcing, precipitation, atmospheric CO₂, relative humidity, and atmospheric deposition of reactive nitrogen species (NO₃⁻, NH₄⁺) under an RCP8.5 climate scenario.

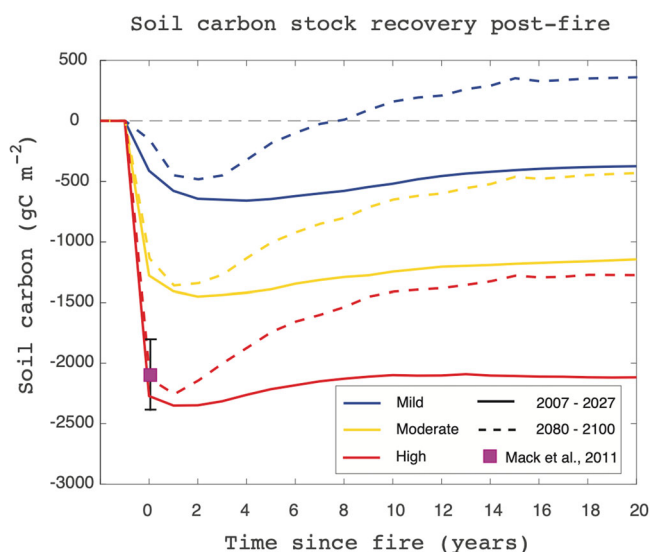


Fig. 3 Total soil organic carbon loss (gC m^{-2}) and recovery trajectory for the period 20 years post-fire. The panel shows both the fire initiated in 2007 (solid lines) and the fire initiated in 2080 (dashed lines). For comparison, the carbon loss measured by Mack et al. (2011), mean \pm standard error, under the actual severe Anaktuvik tundra fire is illustrated, showing very good consistency with the modeled value in the prescribed high-severity fire scenario.

recovery in the case of mild and moderate 2007 fires matched prefire NPP by 2060. The severe-fire NPP remained below prefire levels for the remainder of the 21st Century. In both the early-century fire scenarios, graminoids led the post-fire plant community recovery, and in the year following fires comprised nearly all of the vegetation productivity (Fig. 4b.i, ii). Shrubs re-established more slowly in the case of both early- and late-century fires (Fig. 4b). However, increased rapidly as a proportion of the community in the decades post-fire. Under the early-century fire scenario, shrub expansion occurred earlier than under the RCP8.5-no-fire scenario. The timing of this expansion was dependent on the severity of the fire, with expansion occurring quicker after severe fires. Shrubs, in particular deciduous shrubs, dominated plant community composition by the end of the 21st century. The moss PFT was decimated by the fire, and took nearly 30 years to re-establish as a contributor to community NPP. In the case of the late-century fires, graminoids dominated the reestablished community, while shrubs grew quickly over the next decade.

The transfer entropy approach identified several factors that contributed to the post-fire recovery of community NPP (Supplementary Fig. 3b, c), some of which differed from the factors identified under the baseline RCP8.5 scenario, and differed between the early- and late-century fires. Notably, nutrient availability and uptake is critical for re-establishment of vegetation post-fire (Supplementary Fig. 4). Nutrient availability depends on soil moisture and temperature (particularly in the surface soil), which promotes the activity of several microbial groups decomposing organic matter, thereby liberating nitrogen and phosphorus. Furthermore, nitrogen fixation increases in all cases following fire (see below). For early-century fires, NPP is influenced by snowpack depth and active layer depth, which affects post-fire nutrient cycling. NPP recovery following late-century fire is sensitive to changes deeper in the soil profile, including soil moisture and temperature at depths greater than 0.5 m, indicating that nutrient acquisition that aids NPP recovery occurs from deeper in the soil profile (Supplementary Fig. 4).

Fire effects on 21st century soil moisture and temperature.

ALD deepened by up to 0.2 m in the 8 years following an early century fire (Supplementary Fig. 5). However, over the first two years post-fire the ALD was shallower than the baseline RCP8.5 scenario. Mean annual soil moisture and temperatures also increased, and remained higher than the baseline even as the active layer deepened over the following years (between 2- and 8-years post-fire). These thaw depth dynamics are consistent with data collected at the Anaktuvuk River site post-fire. Modeled soil moisture and temperature maintain dynamic responses for several years post-fire and before stabilizing a decade after a fire (Supplementary Fig. 5a). Indeed, excursions from the RCP8.5 scenario in the ALD, soil moisture, and temperature are also apparent for the next two decades following the fire.

Despite a much deeper active layer by 2080, the onset of fire caused a consistent deepening of ALD (Supplementary Fig. 5b), which continued for two decades following the fire. This deepening was particularly notable under the most severe fire, where ALD deepened 0.2 m by 2100. Much smaller differences between fire severity scenarios were modeled for soil moisture and temperature. However, fire caused annual fluctuations through 2100 in soil moisture and temperature relative to the baseline RCP8.5 scenario.

Fire effects on the 21st century soil microbial community and nutrient cycling.

The simulated changes in vegetation, soil hydrology, and temperature discussed above result in changes in the structure of the belowground microbial community. Notably, fire reduces the abundance of saprotrophic fungi by ~30% between 5 and 20 cm depth, vacating a niche that the fast-growing heterotrophic bacteria fill (Fig. 5). Within warmer, more nutrient-rich shallow (0–5 cm) soils, a long-term change in microbial composition is noted, whereby the heterotrophic bacteria dominate the microbial community over the next century, under both the mild and severe fire scenario (Fig. 6a). However, deeper into the soil profile (~10 cm) heterotrophic bacteria are outcompeted by saprotrophic fungi 10 years post fire (Fig. 6b). The decline in saprotrophic fungi following the end-of-century fire prompts the rapid growth of heterotrophic bacteria taking advantage of the elevated organic matter and nutrient availability (Fig. 5iii/iv). This rapid change in community composition decreases the community C:N ratio from an average of ~8.5 to 6.6, indicative of a microbial community dominated by bacteria (Supplementary Fig. 6). The rapid growth of the heterotrophic bacteria and subsequent SOM decomposition releases inorganic nitrogen and phosphorus (Supplementary Figs. 7b, and 8b), and

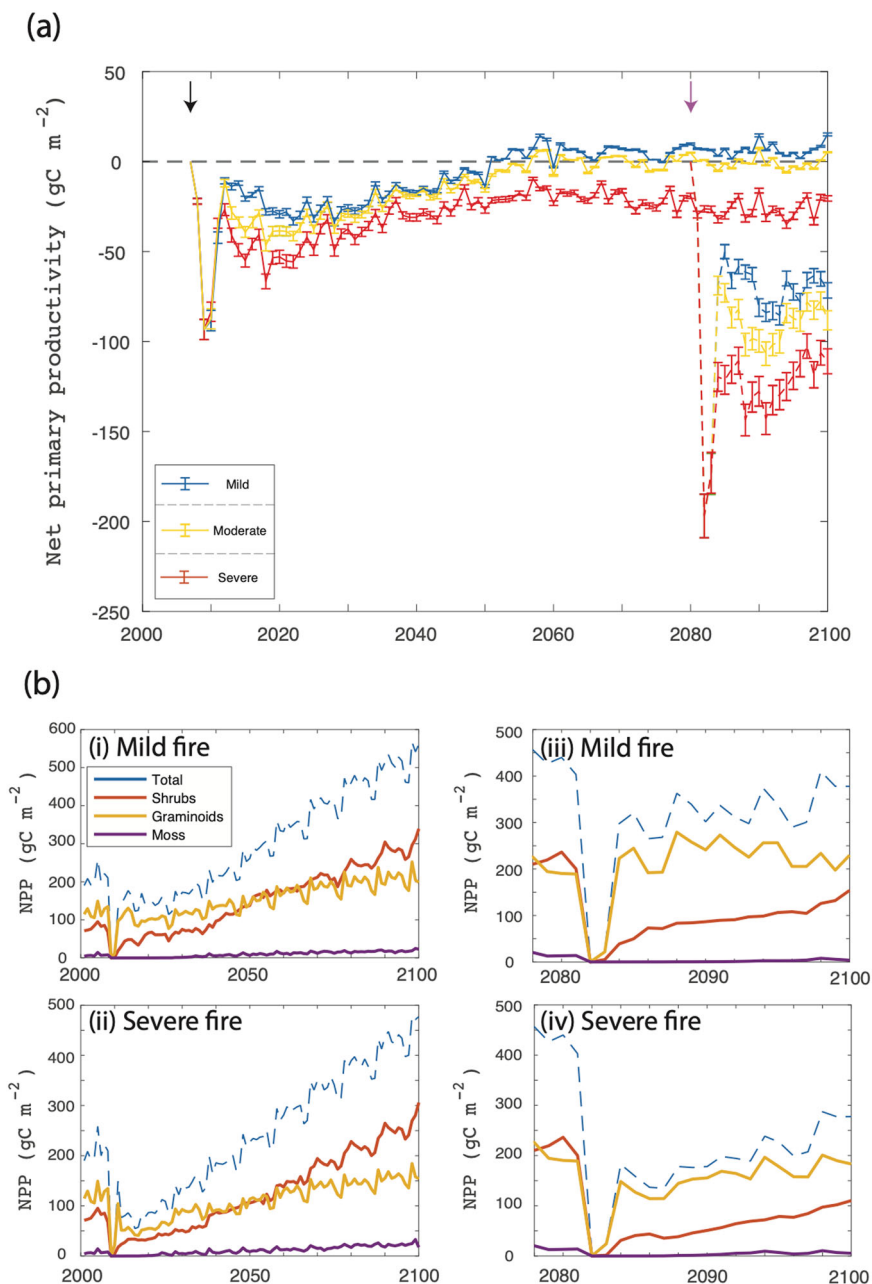


Fig. 4 Net primary productivity ($\text{gC m}^{-2} \text{yr}^{-1}$) post-fire under different scenarios of fire severity and timing. Panels show the total NPP (annual mean \pm standard error) difference from the baseline run under the RCP8.5 scenario. **a** NPP responses under mild, moderate, and severe fires. **b** broken down by plant functional type for (i) a mild, and (ii) severe fire initiated in 2007, and for a (iii) mild and (iv) severe fire initiated in 2080. Changes in PFT NPP for panels (iii) and (iv) cover years 2080–2100 (i.e., the 20 years post-fire).

encourages the growth of autotrophic and heterotrophic organisms involved in nutrient cycling.

Fire creates conditions that lead to ecosystem nutrient losses through Organic matter combustion, NH_3 volatilization and runoff of nitrogen and phosphorus species^{16,52} that would have ordinarily been retained in microbial or plant biomass (Supplementary Figs. 7 and 8). These losses drive selection for microbial groups involved in catalyzing the input and transformation of different nitrogen species, as noted by a post-fire peak in their abundance, in particular in abundance and distribution of diazotrophic bacteria (Fig. 7). Lower nitrogen inventories provide a niche for diazotrophic bacteria capable of fixing atmospheric nitrogen to NH_4^+ . The diazotrophs showed the largest relative increases and spatial colonization, post fire, relative to other

N-cycling groups (Fig. 7). These responses occurred regardless of fire severity or timing of fire onset (i.e., early or late century, Fig. 7). However, fire severity and timing impacted the recovery of nitrogen-fixation post-fire. For example, a mild severity fire early in the century showed a rapid return to prefire nitrogen fixation rates (Supplementary Fig. 9), however, a severe fire at the same time point shows no recovery of nitrogen fixation to prefire levels in the two decades post-fire (Fig. S9b). By contrast, following a severe fire late in the century (ignited in 2080), nitrogen fixation not only recovers quickly but also increases beyond nitrogen fixation rates within unburned soils.

The elevated diazotrophic biomass persisted for longer than both the NH_4^+ - and NO_2^- -oxidizing functional groups. However, in the decades following fire, the biomass of all nitrogen

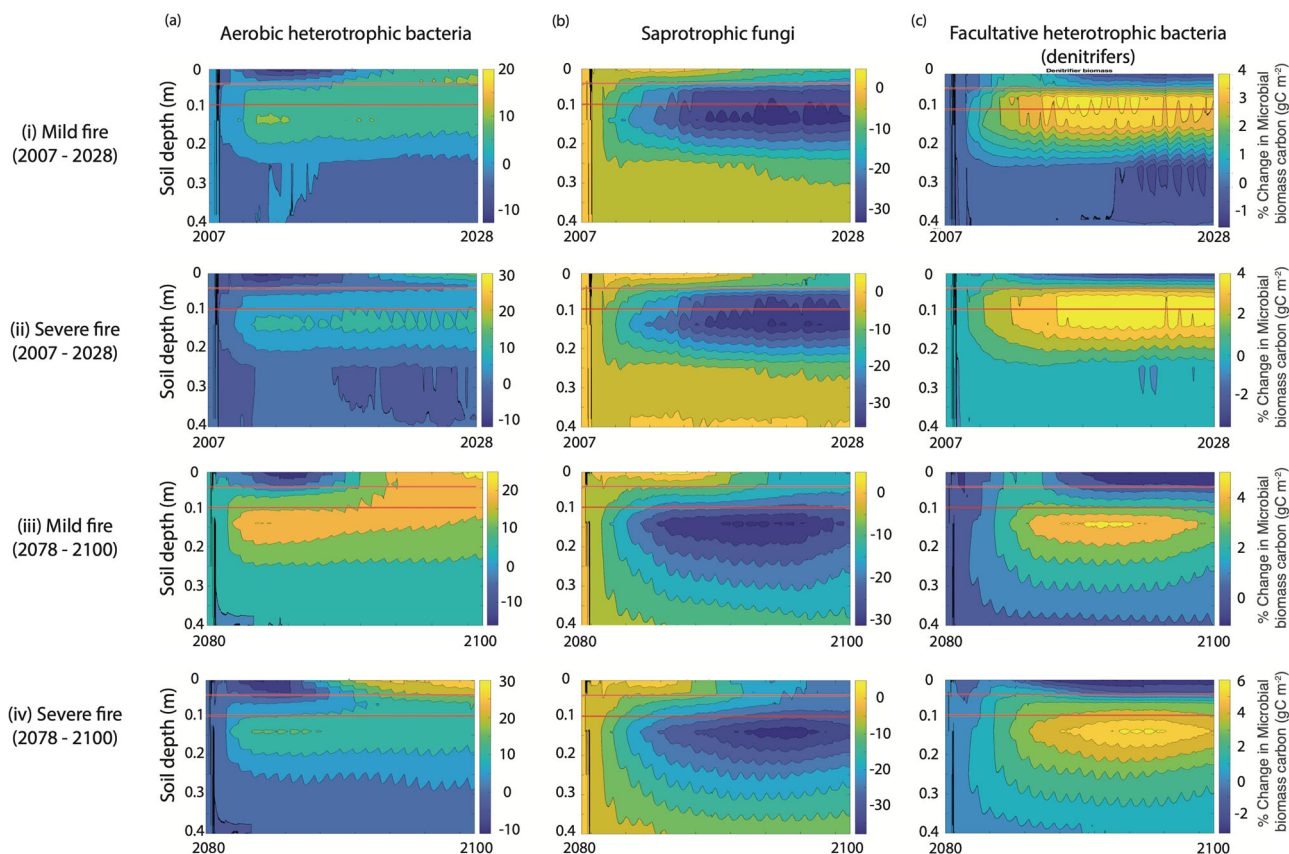


Fig. 5 Long-term trajectory of the heterotrophic community (bacteria + fungi). Percentage change in microbial biomass carbon (each column shows a different microbial functional group) under the four 21st century fire scenarios, and. In the contour plots in columns **a–c**, the colors represent the percent change in microbial biomass relative to the baseline RCP8.5-no_fire simulations. Depicted are the 20 years post fire for (i) the mild fire scenario and (ii) the severe fire scenario between 2007 and 2028, and (iii) the mild fire scenario and (iv) the severe fire scenario between 2078 and 2100. Note: the percentage change color bars are specific to each panel. The red lines in each contour figure represent the depths depicted in Fig. 6.

cycling organisms generally declined (Fig. 7). This trend was consistent with the baseline RCP8.5-no-fire scenario, which showed a decline in biomass of nitrogen-cycling organisms (Fig. 7b). This decline was arrested by the ignition of a late-century fire, which open the niche for nitrogen cycling functional groups. The elevated activity of diazotrophs and soil bacterial heterotrophs increased soil NH_4^+ concentrations (Supplementary Fig. 7b), which stimulated NH_4^+ -oxidation and, in turn, NO_2^- -oxidizing bacteria. The accumulation of NO_3^- is subsequently denitrified, elevating N_2O production (Fig. 8).

Discussion

High-latitude tundra systems face an unprecedented increase in fire frequency and intensity over the 21st Century coupled to ongoing climate warming^{8,53}. Each fire event represents an acute disturbance to the tundra landscape, and leads to large soil carbon losses¹⁵, long-term shifts in vegetation and microbial community composition^{18,20,22,33}, and soil hydrology and temperature. However, the intensification of fire events occurs against a backdrop of ongoing climate change^{54,55}, and the future impact of climate on ecosystem responses to fire disturbances remains a critical knowledge gap. Herein, we used observations from the 2007 fire at Anaktuvuk River, Alaska, as the basis for evaluating model performance and developing model simulations to examine how disturbance from fire affects long-term changes in ecosystem dynamics, soil microbial processes, and tundra carbon cycling. We then use the model algorithms to explore the underlying mechanisms responsible for these dynamics.

Long-term climate responses. In the absence of fire, model simulations predict the site will remain a carbon sink throughout the 21st Century under an RCP8.5 climate scenario. This result is consistent with pan-Alaska⁴³ and pan-Arctic simulations⁵⁶ that, despite regional differences, predict a continuing carbon sink within the Arctic over the next 100 years. These modeled carbon sinks are maintained by a large non-linear increase in NPP over the century, which offsets elevated heterotrophic respiration. The elevated NPP is predominantly attributable to the growth of graminoids and the expansion of shrubs, which become the dominate PFT by mid-century. Shrub expansion is attributable to elevated air temperature and increased soil nutrient availability³⁶. The latter stems from increased organic matter depolymerization and mineralization under warming soils that release both nitrogen and phosphorus⁵⁷. Furthermore, warming and increased soil moisture can deepen the active layer, the latter through increasing thermal conductance⁴² and precipitation heat content⁴⁴. A deepening active layer can enhance microbial decomposition of newly accessible organic matter⁵⁸ and release previously frozen inorganic and organic nutrients, which can be assimilated by tundra plants^{59–61} directly and through mycorrhizal symbionts⁶². Indeed, nutrient uptake from permafrost soils has previously been shown to promote a shift in community composition from graminoid-dominated towards shrub-dominated ecosystems⁶³.

The expansion of shrubs across tundra ecosystems is consistent with both observational evidence^{34,35,64} and model simulations⁴⁹. At the northern Anaktuvuk River site, evergreen shrubs were observed and modeled to be significant contributors to ecosystem biomass and NPP at the beginning of the 21st century and after the

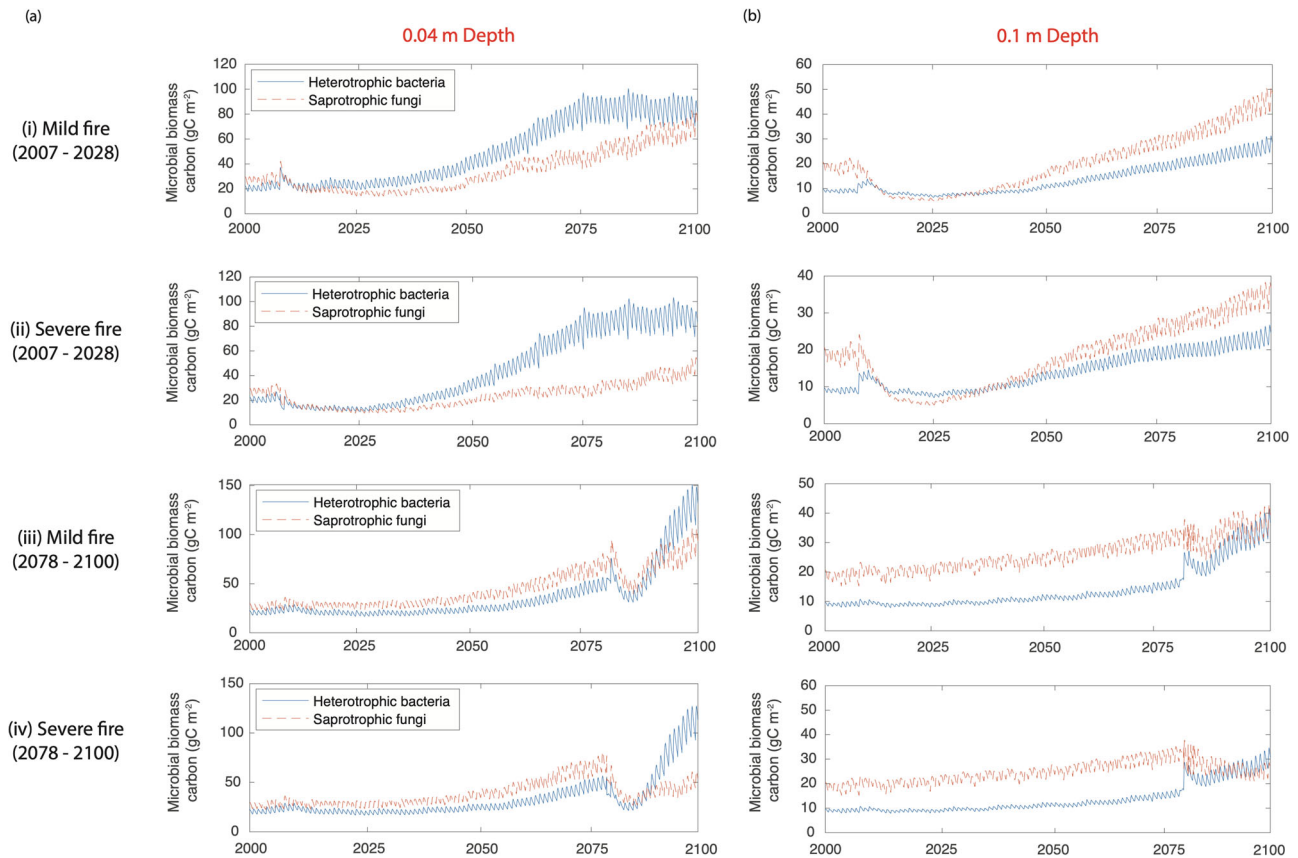


Fig. 6 Changes in heterotrophic bacterial and saprotrophic biomass over time. This figure provides the trajectory of microbial biomass (gC m^{-2}) at two different depths, **a** 4 and **b** 10 cm between 2000 and 2100, respectively. As for Fig. 5, depicted are the 20 years post fire for (i) the mild fire scenario and (ii) the severe fire scenario between 2007 and 2028, and (iii) the mild fire scenario and (iv) the severe fire scenario between 2078 and 2100.

onset of wildfire¹⁷. The initial simulated evergreen shrub expansion is consistent with recent studies^{65,66}, and could be attributable to relatively low post-fire nutrient availability, which favors the more conservative strategy of evergreen shrubs^{36,67}. In *ecosys*, evergreen shrub traits imply a more conservative PFT that are slower growing and have slower leaf turnover. In contrast, deciduous shrubs have more rapid leaf turnover, higher nutrient uptake capacity, and more efficient nutrient remobilization, all of which produce competitive advantages under more nutrient rich conditions. Over time, post-fire nutrient cycling accelerates and taller deciduous shrubs increase in abundance, driving shrub expansion, consistent with recent observational²⁴ and simulation studies⁴⁹.

Long-term climate–fire interactions. Measured and modeled post-fire recovery of the plant community occurred rapidly. Graminoids, in particular, recover rapidly following fire, almost reverting to prefire NPP a few years later. While the lack of competition from evergreen and deciduous shrubs likely facilitates this recovery, increased nitrogen and phosphorus availability immediately following the fire alleviates nutrient limitation, at least temporarily, allowing for quicker recovery of PFTs possessing traits that lead to more rapid nutrient uptake and thereby growth. This mechanism has support from measurements following the Anaktuvuk River site fire¹⁷ and observed initial increases in graminoid abundance within nutrient fertilization experiments⁶⁸. Shrubs take longer to re-establish in the years following fire relative to graminoids. However, for severe fires occurring earlier in the century, enhanced shrub growth (i.e., evergreen + deciduous shrubs) was modeled to occur approximately a decade earlier than under the RCP8.5-no_fire scenario,

and notably, shrub growth is far quicker towards the end of the century. Under the RCP8.5-no_fire scenario, shrubs contribute more to community NPP than graminoids by 2100 (52% from shrubs, 44% from graminoids). By contrast, after the onset of a severe fire early in the century, shrubs contribute 70% of community NPP, relative to 28% contributed by graminoids by 2100. The mild-severity fire also resulted in enhanced shrub expansion, and by 2100, the contribution of shrubs to community NPP increased relative to graminoids (59% from shrubs, 39% from graminoids) under the early-century fire severity scenario. Similar responses in shrub expansion have previously been observed following tundra fire under similar conditions to those modeled here^{8,22}.

The factors influencing modeled NPP recovery show commonalities between fires of different severity occurring over the same time period (i.e., either at the beginning or the end of the 21st century). The most important variables supporting NPP recovery, as identified by our information entropy approach, include soil moisture content, nutrient availability, and plant nutrient assimilation (Supplementary Fig. 4). While these factors are likely coupled, nutrient availability is a strong control on primary productivity in tundra communities^{68,69}. A large loss of nutrients, which can occur post-fire as a result of combustion, increased run-off, or volatilization^{16,70,71}, can slow ecosystem recovery within these nutrient limited systems. We modeled large dissolved inorganic nitrogen losses, primarily in post-fire runoff, alongside more moderate concentrations of dissolved organic nitrogen. How ecosystems reestablish nutrient cycling post-disturbance is critical to the recovery of ecosystem function and maintaining a balance between plant assimilation and microbial transformation⁷².

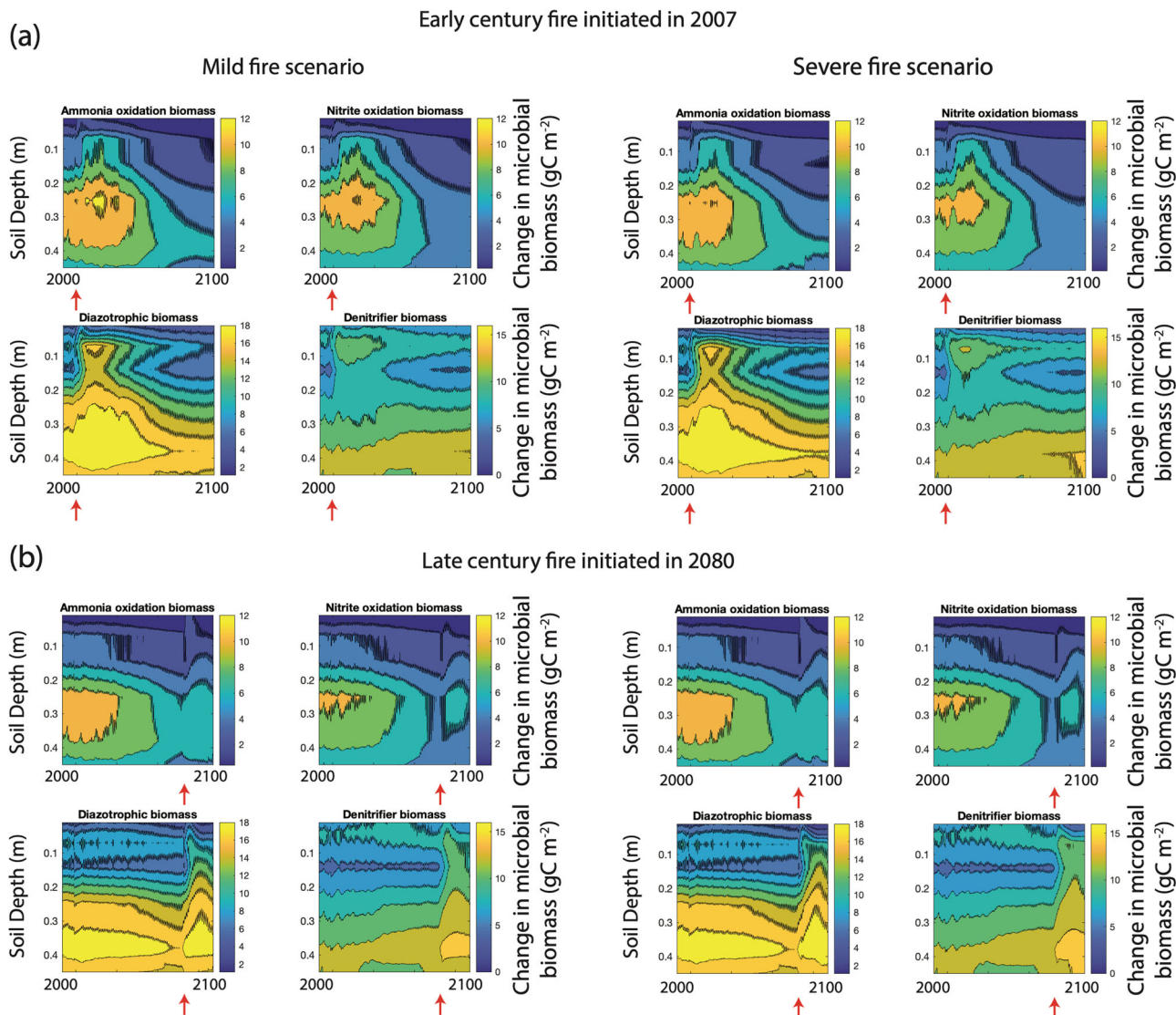


Fig. 7 Fire impacts on nitrogen cycling microbes. Changes relative to the baseline RCP8.5-no_fire scenario in the biomass (gC m^{-2}) of nitrogen cycling organisms, NH_4^+ and NO_2^- oxidizers, facultative denitrifying bacteria, and diazotrophic bacteria under different fire scenarios for the period spanning 2000–2100. Panels show the same depth range (0–0.45 m) and temporal scale (2000–2100) for the mild fire severity (left side), and the severe fire (right side panels). Panels depict **a** biomass of four microbial functional groups over the century for a fire ignited in 2007, **b** microbial biomass over the RCP8.5 simulations until the onset of fire in 2080. Red arrows along the x-axis indicate the year fire was initiated. The biomass of each organism represents the difference between the total microbial biomass over time.

The role of belowground communities in ecosystem recovery. Several studies have developed conceptual theories concerning ecosystem recovery from disturbance^{72–74}. For example, Rastetter et al.⁷², identify three distinct phases in ecosystem recovery that are underpinned by nutrient availability. This framework encompasses the transition through quasi-steady states post-disturbance toward a steady state. The initial recovery is largely dependent on the openness of the nutrient cycles, which determines the proportion of nutrients passed from soils to vegetation rather than being exported.

Our simulations show that hydrological and gaseous nitrogen losses are at their highest in the years after fire disturbance, indicating an open nitrogen cycle in the absence of vegetation. This dynamic is consistent with the first stage of ecosystem recovery⁷² whereby vegetation assimilation remains low during regrowth. A more open nitrogen cycle is also consistent with observations of nutrient export made at burned and unburned regions across the Anaktuvuk site⁷⁰. Combustion of aboveground

and belowground biomass diminishes competition between vegetation and the microorganisms that rapidly colonize the burned soils. In the years following fire, bacterial heterotrophs (i.e., aerobic + facultative) dominate OM mineralization after most of the saprotrophic fungi is burned away. This successional pattern has ramifications for the rate of carbon and nutrient cycling. In *ecosys*, relative to the fungal saprotrophs, bacterial heterotrophs have faster growth rates and a lower C:N biomass, resulting in a higher rate of OM turnover and lower necromass contribution to organic matter accumulation. These modeled traits also facilitate the heterotrophic competitive advantages early in succession. Such a shift is consistent with a recent conceptual framework that hypothesizes consistency between plant and microbial responses to fire, notably with an initial post-fire colonization by fast-growing bacteria⁷⁵.

Vegetation recovery following fire is facilitated by nitrogen and phosphorus made available by bacterial heterotrophic mineralization of existing soil organic matter. In nitrogen-limited

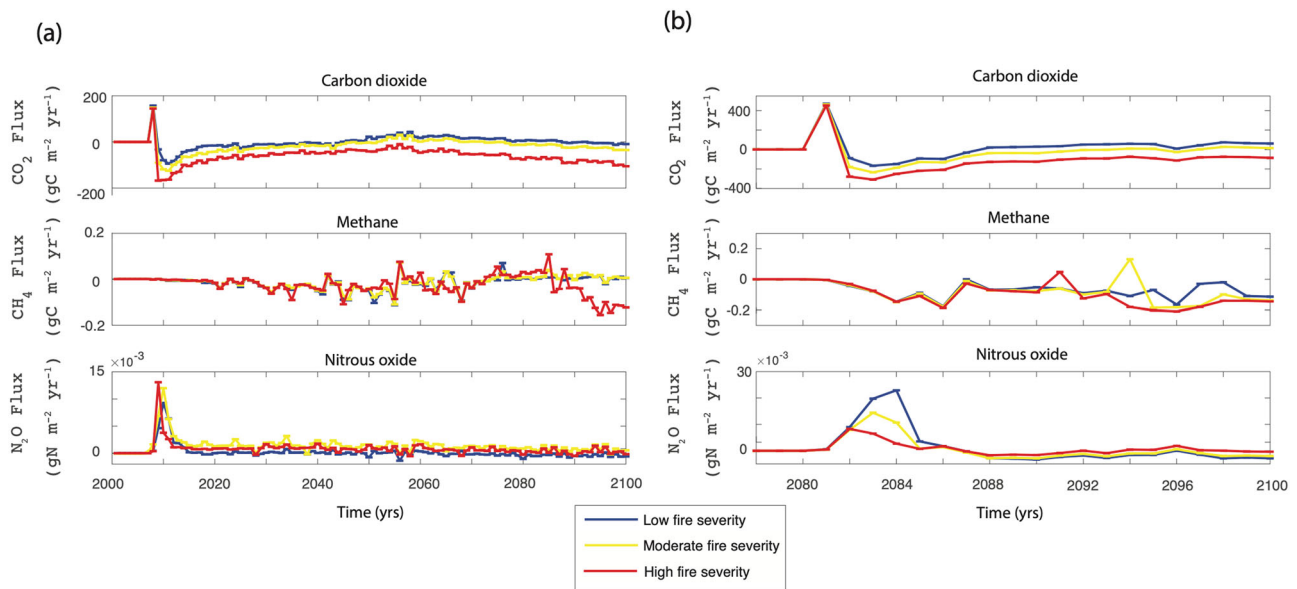


Fig. 8 Trace gas fluxes under the various fire scenarios. Gas fluxes (CO₂, N₂O, CH₄, annual mean \pm standard error) were normalized to the baseline RCP8.5-no_fire simulation to highlight the impact of fire for **a** early-century fire (ignited in 2007), and **b** late-century fire (ignited in 2080). Note that the timescales for panels **a** (years 2000–2100) and **b** (years 2075–2100) are different. Note: positive values for gas fluxes represent emissions from the soil.

tundra, with low inputs through atmospheric deposition and nitrogen fixation⁷⁶, recycling of organic matter and release of inorganic nutrients is the dominant pathway through which nutrients are made available for plant assimilation⁷⁷. Diazotrophic microorganisms also respond rapidly following fire, increasing in biomass across the soil profile. However, nitrogen fixation remains far too low to account for the large modeled increase in soil nitrogen post-fire, and annual rates of nitrogen fixation are approximately two orders of magnitude lower than the post-fire peak in NH₄⁺ availability. This is consistent with recent observations^{78,79} that conclude that nitrogen fixation is a minor contributor to balancing the nitrogen cycle after tundra disturbances. In our simulations, diazotrophic abundance increased following fire because of their facultative capabilities. While diazotrophs are modeled to fix nitrogen when it is scarce, they retain the capacity to take it up from the surrounding environment when available⁸⁰. Following fire, modeled diazotrophs benefit from reduced competition for nitrogen from plants and fungi, and expand their niche by fixing nitrogen while also assimilating available NH₄⁺ following mineralization.

Increasing NH₄⁺ concentrations post-fire also stimulates nitrification, increasing the production of more mobile NO₃⁻. NO₃⁻ accumulation in the soil is ephemeral because it is rapidly lost hydrologically and subject to uptake by tundra plants⁸¹. Observations support the modeled increase in nitrification rates following fire^{82–84}. Our simulations also suggest a long-term disturbance to the nitrogen cycle, whereby nitrification is elevated for several decades following fire, consistent with observations from ecosystems that are not adapted to stand-replacing fires⁸³. The drop in nitrifying microbial biomass occurs as competition for NH₄⁺ increases concomitant with vegetation growth, as the ecosystem transitions towards a quasi-steady state as nutrient cycles close, and a balance between plant assimilation and microbial immobilization is reached.

Ecosystem response to early-century fire. Despite a modeled NPP recovery following fire consistent with observations¹⁷, the full recovery of vegetation NPP and biomass takes several decades under mild fire conditions, and did not fully recover under the severe early-century burn scenario by 2100. This impact on

vegetation is reflected in the soil carbon stocks, which do not recover to pre-disturbance levels by 2100 under all modeled early-century fire severity scenarios. This is consistent with previous studies simulating the soil carbon response to the ANF⁸⁵. Soil nutrient accumulation post-fire continues over the century; however, nitrogen concentrations remain lower than under the climate-only scenario, showing that fire results in a long-term deficit of nitrogen. Furthermore, tundra ecosystems continue to lose inorganic nitrogen hydrologically over the century following a severe fire (Supplementary Fig. 7). These results suggest that a steady state in nitrogen balance takes more than a century to attain for these ecosystems, although the modeled increases in inorganic nitrogen losses later in the century also interact with warming increased decomposition rates and nutrients losses. Indeed, Mack et al.¹⁵, estimated that the Anaktuvuk River fire caused the loss of 400 years of accumulated ecosystem nitrogen. Our simulations show that replenishment of such nitrogen stocks could be further compromised by a warming climate.

Ecosystem response to late-century fire. The ecosystem that burns in 2080 is notably different from the 2007 landscape in two main regards. First, as discussed earlier, shrub abundance (in terms of contribution to total biomass and NPP) increased over the century, and is slightly higher relative to the graminoids by 2080. Second, and related to the elevated shrub abundance, soil nitrogen and phosphorus concentrations are significantly higher by 2080. Large increases in soil nutrient concentrations stem from several pathways. First, the mineralization of organic matter within the shallow soil is enhanced by increasing soil and air temperatures^{86,87}. Second, modeled abrupt deepening of the ALD after 2060 exposed ancient organic matter previously sequestered in permafrost, which can be rapidly mineralized, yielding nutrients that are available for plant uptake⁵⁹. Third, the model predicts an increasing snowpack depth over the century, and the resulting higher winter soil temperatures (from ~ -9 °C in 2000 to ~ 0 °C in 2080) encourage microbial growth and activity throughout the winter time, which has previously been shown to be an important time period for the release of nutrients^{88,89} and uptake by plants⁹⁰. In addition to faster, more open nutrient cycles in the late 21st Century, a notable relative decline in soil

moisture occurs ~3 years following fire, which permits further oxygenation of the soil, thereby increasing microbial activity⁹¹. The accelerated nitrogen cycle that emerges towards the end of the century and higher availability of inorganic nitrogen leads to larger N₂O emissions post-fire. The highest N₂O emissions (1.3×10^{-2} gN m⁻²) occur under a mild fire scenario (Fig. 8b), which limits the combustion of the microbial community and leads to a prolonged period of wetter soil, creating a niche for denitrifying organisms.

The higher prefire nutrient concentrations at the end of the century partly explain the more rapid recovery of the vegetation community to disturbance. Under these circumstances, an equilibrium between microbial immobilization and vegetation nutrient demand is reached quickly, facilitating the restoration of soil carbon stocks following a mild fire within two decades. Plant communities following fire are dominated by graminoids, with a slower recovery of shrub communities. Compared with the early-century simulations, shrubs increase more rapidly as a proportion of the total vegetation community the decade following a fire due to elevated nutrient availability selecting for plants with higher nitrogen use efficiency, allowing for higher carbon fixation relative to nitrogen uptake.

Conclusion. The simulations presented here clearly show microbially-dependent nutrient controls on the recovery of tundra ecosystems and progression of community development post-fire. These microbial and plant successional trajectories are strong functions of competitor dynamics represented in *ecosys*. The ramifications of early-century fire persist for several decades post-fire and shape vegetation community development and the balance of nutrient losses and retention. However, over the next century, tundra warming will likely accelerate soil nutrient cycling, increasing nutrient availability, and hastening ecosystem recovery. Ignoring microbial dynamics, and plant-microbe interactions, likely increases the uncertainty of tundra carbon cycle interactions with climate change.

The outbreak of fire within the tundra of the North Slope of Alaska is an extremely rare event^{15,46}. Indeed, there is little evidence for fire in this region over the previous 6000 years^{53,92}. However, tundra fire return intervals are predicted to increase over the next century⁵³. A combination of interrelated factors appears responsible for an increasing rate of return, including the declining extent of sea-ice coverage⁴⁶, increasingly warm and dry grow seasons⁴, and the elevated frequency of lightning strikes⁸ largely responsible for tundra wildfires¹¹. How communities recover post-wildfire depends upon this rate of return, which can shape the distribution of fire-resistant traits within plant⁹³ and, potentially, microbial communities⁹⁴. However, recovery is also dependent on ecosystem nutrient retention and recycling post-fire, which enables plant growth. Our simulations show full recovery of plant productivity within four decades of the ANF event, and this recovery could be quicker still²⁴. This indicates that aboveground communities recover rapidly albeit with an alternative stable state in which shrubs increasingly dominate the successional community. By contrast, belowground recovery is much slower, particularly following severe fires. Modeled carbon stocks take many decades to recover, consistent with empirical estimates¹⁵. Increasing the rate of wildfire return within these systems could further undermine the stability of these organic matter stocks, reducing the available organic matter that is a large source of available nutrients, and reduce the efficacy of recovery of aboveground systems.

Materials and methods

Site description. The model (described below in detail) was parameterized and benchmarked against data derived from one of the largest tundra fires in recent

record, the Anaktuvuk River Fire (ANF)^{15,17}. Anaktuvuk River is located on Alaska's North Slope (68.5838°N, 149.7178°W), and is underlain by continuous permafrost. The mean annual temperature is -10 °C, with a range of -15 °C in winter to 12 °C in summer, which the mean annual precipitation is ~30 cm, with a third falling as snow¹⁵. The ANF was ignited by a summer lightning strike in July 2007^{23,47}. Several factors, including record high temperatures, and record low rainfall contributed to the size and severity of the fire. The fire burned 1039 km² of tundra, with 80 % being of moderate to severe burn^{15,47}.

Model description and set-up. To address the preceding questions we apply a well-tested mechanistic ecosystem model, *ecosys*, which simulates the inter-dependent physical, hydrological, and biological processes that govern ecosystem responses to perturbation. The model, which includes mechanistic representations of carbon, water, nitrogen, and phosphorus dynamics in plants and soils, has been successfully applied in dozens of sites around the world, with many studies focusing on high-latitude ecosystems^{41–45}. In brief, *Ecosys* is an hourly time-step land model with multiple canopy and soil layers and fully coupled carbon, energy, water, and nutrient cycles solved at an hourly time step. Surface energy and water exchanges drive soil heat and water transfers to determine soil temperatures and water contents. These transfers drive soil freezing and thawing and, hence, active layer depth, through the general heat flux equation. Carbon uptake is controlled by plant water status calculated from convergence solutions that equilibrate total root water uptake with transpiration. Atmospheric warming increases surface heat advection, soil heat transfers, and hence active layer depth. Finally, *ecosys* represents prognostic dynamics of permafrost and its effects on active layer hydrology driven by basic processes for transfer and transformation of energy and water, and acclimation of all biological processes to warming.

Below we outline some of the model features that are pertinent to the current study.

Microbial community structure. Microbial communities are represented in *ecosys* as eleven distinct functional groups across each modeled soil layer^{95–97}. The composition of the microbial community is affected by competition between the functional groups, which represent a collection of different traits related to substrate acquisition and the thermodynamics of different metabolisms. Aerobic heterotrophic bacteria and saprotrophic fungi couple decomposition of the DOC pool to O₂ as a primary electron acceptor, which drives heterotrophic respiration (R_h). R_h can be constrained by soil temperature and soil water content (see below), O₂ and substrate availability, and microbial stoichiometry (C:N:P). The microbial groups undergo maintenance respiration (R_m) dependent on microbial stoichiometry (C:N) and soil temperature. R_h in excess of R_m is used in growth respiration (R_g), whereby the energy yield (ΔG) drives the growth of biomass (M) from substrate uptake according to the energy requirements of biosynthesis. Finally, microbial mortality (D_m) occurs either under a first order decay rate, and when R_m is in excess of R_h . Microbial biomass (M) is determined by the difference between DOC uptake and loss from R_m , R_g , and D_m .

Alternative electron acceptors are also represented in the model, whereby R_h not coupled to O₂ proceeds through the sequential reduction of nitrate (NO₃⁻) to gaseous nitrogen (N₂) (i.e., denitrification: NO₃⁻ → NO₂⁻ → N₂O → N₂), or the reduction of organic carbon through fermentation or acetotrophic methanogenesis. Of these anaerobic bacteria, the denitrifying bacteria are represented as facultative anaerobes (i.e., able to utilize both O₂ and reduced N compounds as electron acceptors). The rate limiting step of the redox nitrogen cycle is represented as a two-step chemolithoautotrophic reaction whereby ammonium (NH₄⁺) is oxidized to nitrite (NO₂⁻), which is oxidized to NO₃⁻. N₂O is a potential byproduct of this pathway under circumstances where the two components of the reaction are uncoupled. The NH₄⁺ that initiates the nitrogen cycle is provided through new sources of N, atmospheric deposition or nitrogen fixation, or recycled nitrogen from organic matter (OM) mineralization. Free-living diazotrophs are represented by both aerobic and anaerobic bacteria, which allocate R_g partially towards the fixation of atmospheric N₂. Methane (CH₄) production and oxidation are represented in the model by hydrogenotrophic and acetoclastic methanogens and chemolithoautotrophic methane oxidizers.

Within the soil environment all microbial groups seek to maintain minimal stoichiometric ratios (i.e., C:N or C:P) through the mineralization and uptake of dissolved organic nitrogen, and phosphorus, NH₄⁺, NO₃⁻, and H₂PO₄⁻, thus competing with plant roots and mycorrhizal uptake and affecting soil solution concentrations of these compounds. Free-living diazotrophs fix aqueous N₂ under conditions where assimilation of N-compounds is insufficient to maintain their minimal C:N⁸⁰.

OM in each soil layer is represented by several OM-microbial complexes of various thermodynamic favorability and availability to microbial heterotrophs⁹⁸. Of particular relevance to this study are the two SOM pools denoted "active" and "passive". The active pool is further resolved into components of variable thermodynamic potential; protein, carbohydrate, cellulose, and lignin. The passive SOM pool represents mineral-OM interactions, and is divided into two pools representing compounds reversibly sorbed onto mineral surfaces⁹⁹, and those stabilized onto surfaces. Sorption to mineral surfaces is calculated by a Freundlich isotherm. Microbial decomposition products (e.g., C, N, or P) from organic matter-microbial complexes are gradually stabilized into more recalcitrant organic

compounds with lower C:N and C:P ratios. Products from lignin hydrolysis combine with some of the products of protein and carbohydrate hydrolysis in the litterfall and are transferred to the particular organic matter complex.

The parameter values for each group are provided in Supplementary Material, however, in qualitative terms heterotrophic bacteria growing on simple DOC compounds while using O_2 as an electron acceptor generally increase in biomass faster than other bacteria due to a larger energy yield from the redox reaction. By contrast, facultative anaerobes such as denitrifiers grow at a slower rate than obligate aerobes when using O_2 as an electron acceptor, due to intracellular trade-offs that permit growth coupled to the reduction of different nitrogen compounds. Fungi show similar thermodynamic energetics to heterotrophic bacteria in terms of decomposition of organic compounds using O_2 as an electron acceptor, but a slightly lower efficiency of biomass production, and a higher metabolic stoichiometry¹⁰⁰.

Finally, in addition to soil nutrient availability, the growth and activity of the microbial functional groups are further constrained by soil temperature and soil water content⁹⁷. Microbial substrate hydrolysis and oxidation by heterotrophic groups is sensitive to soil temperature according to a modified Arrhenius function with upper and lower temperature constraints⁹⁷.

Plant functional types. *Ecosys* represents multiple canopy and soil layers allowing for mechanistic Plant Functional Type (PFT) competition for light, water, and nutrients. The model represents various PFT traits that are distinct between plants, including specific leaf area, leaf clumping, turnover, optical properties, foliar nutrient content and retention, and root hydraulic conductivity⁴⁰. Differences in growth rate and nutrient acquisition and conservation strategies drive different competitive strategies, through differential allocation of non-structural carbon, nitrogen, and phosphorus to different plant organs dependent on PFT⁴⁵. This allocation determines leaf area, canopy height, and belowground allocation patterns, which, in turn, determine interception of direct and diffuse radiation across each canopy layer, and competition for nutrients and water through allocation to roots, which shapes their length and density. Nutrient competition is further influenced by belowground allocation to mycorrhizal fungi. Most PFTs engage fungal partners, many explicitly as mycorrhizae, which exchange soil nutrients (e.g., N and P) for photosynthetic carbon. Mycorrhizae have larger surface area to volume ratios than plant roots, enabling greater uptake of soil nutrients and water.

The collection of traits determines competition between different PFTs for light and nutrients through the allocation and investment of carbon in leaves, stems, and roots. Four PFTs are represented in the current study based on previous observations from the Anaktuvuk River site: graminoids (similar to *Eriophorum vaginatum*), evergreen shrubs (*Ledum palustre*), deciduous shrubs (*Betula nana*), and nitrogen-fixing mosses (*Hylocomium splendens*). A full account of the different traits associated with these PFTs has been published recently⁴⁰. Briefly, the deciduous shrubs are represented as having a greater specific leaf area and lower leaf clumping than evergreen shrubs, leading to greater light interception. The deciduous shrubs all have full annual leaf turnover, whereas evergreen shrubs retain their leaves year-round. Nutrient conservation under litterfall is driven by carbon, nitrogen, and phosphorus recycling coefficients, which increase with non-structural C:N ratios⁴⁵. Higher nutrient remobilization (N and P) is modeled for evergreen shrubs relative to deciduous shrubs, allowing evergreens to better compete in nutrient limited environments^{50,67}.

Evergreen shrubs are represented as the most conservative PFT, with a relatively slow water uptake due to higher axial hydraulic resistance, slower leaf turnover, and slower plant growth. By contrast, deciduous shrubs have faster nitrogen and water uptake, due to a lower axial resistivity, resulting in a less conservative and more rapid growth strategy relative to evergreen shrubs^{40,67}. Deciduous shrubs are also better competitors under more nutrient rich conditions, but have a more rapid leaf turnover. However, the leaf nutrient concentrations are dynamic and dependent on nutrient availability, which feeds back onto modeled carboxylation rates and electron transport. Greater investment in nutrient uptake drives higher CO_2 fixation rate in deciduous, relative to evergreen, shrubs³⁶.

Model initialization and testing. We first initialized the model at the Anaktuvuk River site using published data for soil and vegetation properties^{15,17,23,47}. Eleven soil layers were represented to a depth of 2 m. Soil properties across the soil layers were initialized with attributes from the Unified North America Soil Map¹⁰¹, and measured site specific values for edaphic factors (bulk density, soil pH, sand, silt and clay content, depth to groundwater^{15,23}) and vegetation¹⁷. Soil organic carbon was initialized with the Northern Circumpolar Soil Carbon Database¹, with additional input from recent publications¹⁵.

It should also be noted that a recent application of *ecosys* at a tundra site in Utqiagvik, Alaska, USA (71.3°N, 156.5°W) showed concordance between modeled and observed processes (Grant et al.¹⁰²), including CO_2 ($R^2 = 0.7-0.9$) and CH_4 ($R^2 \sim 0.9$) fluxes, LAI (|bias| = 0.01–0.35 m² m⁻²), and plant biomass (|bias| = 0.08–19.6 gC m⁻²); landscape-scale latent ($R^2 = 0.71-0.77$), and sensible ($R^2 = 0.78-0.88$) heat fluxes; soil temperatures ($R^2 = 0.92$); active layer depth (RMSE = 2–5 cm), and soil moisture (RMSE = 0.05–0.09 m³ m⁻³). We also analyze 25 km resolution simulations across the North America (NA) tundra in which *ecosys* accurately reproduced observed inter-annual variability in LAI spatial patterns ($R^2 = 0.71$), long-term mean annual GPP ($R^2 = 0.78$) (41), and active layer

depth from 28 Circumpolar Active Layer Monitoring sites ($R^2 = 0.63$; RMSE = 10 cm) (Mekonnen et al.⁴⁴).

Model simulations. To produce a realistic starting ecosystem state, spin-up simulations were run from 1900 to 2000 under dynamic climate, atmospheric CO_2 concentrations¹⁰³, and nitrogen deposition¹⁰⁴. The atmospheric forcing data (i.e., air temperature, precipitation, downward shortwave radiation, relative humidity, and wind speed) for each site were taken from the North American Regional Reanalysis (NARR), a long-term weather dataset originally produced at the National Oceanic and Land Administration (NOLA) National Centers for Environmental Prediction (NCEP) Global Reanalysis¹⁰⁵. Where possible these model drivers were supplemented by site-specific data. The fire and climate perturbations, starting in 2000 following spin-up, were derived from the representative concentration pathways 8.5 (RCP8.5) scenario obtained from ensemble projections, downscaled and averaged from 15 CMIP models. RCP8.5 is broadly consistent with global emissions between 2006 and 2017. Fire disturbances were prescribed either in 2007 or 2080 during the RCP8.5 scenario (Table 2). The modeled depths of burn and extent of organic matter combustion for six fire severity scenarios were taken from a previously published dataset⁵¹ (Table 2).

Statistical analysis. The correlation between observational benchmarks and site simulations were assessed using a root mean square error test. Significant differences between variables (e.g., changes in soil carbon, net primary productivity, etc.) were tested using an analysis of variance test. Finally, we used an information theory approach (transfer entropy⁴⁹), to examine directional impacts from one variable (e.g., soil nutrient cycling) to another (e.g., net primary productivity). These relationships were inferred by Shannon information entropy (H) and its transfer (TE) (unit bits), as previously described¹⁰⁶.

$$H = - \sum_{i=1}^n p(x_i) \log_2 p(x_i)$$

$$T_{X \rightarrow Y} = \sum_{y_i, y_{i-1}, x_{i-j}} p(y_i, y_{i-1}, x_{i-j}) \log_2 \frac{p(y_i | y_{i-1}, x_{i-j})}{p(y_i | y_{i-1})}$$

where $p(x)$ is Probability Density Function (PDF) of x , $p(y_i, y_{i-1}, x_{i-j})$ is the joint PDF of the current time step y_i , previous time step of y_i , and j th time step before x_i , $p(y_i | y_{i-1}, x_{i-j})$ and $p(y_i | y_{i-1})$ denote conditional PDF of the corresponding variables. For example, the information entropy transfer from plant photosynthesis processes to soil heterotrophic respiration processes (R_H) is then calculated as Shannon entropy reduction (uncertainty reduction) of present R_H given the historical net primary productivity (NPP) records and also excluded the influence from previous time step R_H . The significant threshold of transfer entropy from GPP to R_H is identified by first randomly shuffling NPP and R_H time series, then calculating the shuffled transfer entropy, assuming the randomly shuffled breaks the dependency between NPP and R_H . Variables included in this analysis are NPP, nutrient concentrations (NH_4^+ , NO_3^- , PO_4^{3-}), plant nutrient uptake, soil carbon concentration, total microbial biomass, aerobic heterotrophic biomass (0.1 and 0.5 m), saprotrophic biomass (0.1 and 0.5 m), air temperature, soil temperature, soil moisture content (0.1, 0.5, 0.85 m), active layer depth, and snowpack depth.

Data availability

The model runs, and scripts used to generate the figures and analyze the data are publicly available at the ESS-DIVE repository (<https://ess-dive.lbl.gov/>) at <https://doi.org/10.15485/1670465>.

Code availability

The *ecosys* model is available for download, <https://github.com/jinyun1tang/ECOSYS>.

Received: 19 July 2021; Accepted: 20 January 2022;

Published online: 11 February 2022

References

- Hugelius, G. et al. A new data set for estimating organic carbon storage to 3 m depth in soils of the northern circumpolar permafrost region. *Earth Syst. Sci. Data* 5, 393–402 (2013).
- Hugelius, G. et al. Estimated stocks of circumpolar permafrost carbon with quantified uncertainty ranges and identified data gaps. *Biogeosciences* 11, 6573–6593 (2014).
- Mishra, U. et al. Spatial heterogeneity and environmental predictors of permafrost region soil organic carbon stocks. *Sci. Adv.* 7, eaaz5236 (2021).
- Serreze, M. C. & Barry, R. G. Processes and impacts of Arctic amplification: a research synthesis. *Glob. Planet. Change* 77, 85–96 (2011).
- Xiao, J. & Zhuang, Q. Drought effects on large fire activity in Canadian and Alaskan forests. *Environ. Res. Lett.* 2, 044003 (2007).

6. Higuera, P. E. & Abatzoglou, J. T. Record-setting climate enabled the extraordinary 2020 fire season in the western United States. *Glob. Change Biol.* 15388 <https://doi.org/10.1111/gcb.15388> (2020).
7. Ziel, R. H. et al. A comparison of fire weather indices with MODIS fire days for the natural regions of Alaska. *Forests* **11**, 516 (2020).
8. Chen, Y. et al. Future increases in Arctic lightning and fire risk for permafrost carbon. *Nat. Clim. Chang.* <https://doi.org/10.1038/s41558-021-01011-y> (2021).
9. Holloway, J. E. et al. Impact of wildfire on permafrost landscapes: a review of recent advances and future prospects. *Permafrost. Periglacial Process* pp. 2048 <https://doi.org/10.1002/ppp.2048> (2020).
10. Kim, J.-S., Kug, J.-S., Jeong, S.-J., Park, H. & Schaepman-Strub, G. Extensive fires in southeastern Siberian permafrost linked to preceding Arctic Oscillation. *Sci. Adv.* **6**, eaax3308 (2020).
11. Veraverbeke, S. et al. Lightning as a major driver of recent large fire years in North American boreal forests. *Nat. Clim. Change* **7**, 529–534 (2017).
12. Rocha, A. V. et al. The footprint of Alaskan tundra fires during the past half-century: implications for surface properties and radiative forcing. *Environ. Res. Lett.* **7**, 044039 (2012).
13. Iwahana, G. et al. Geomorphological and geochemistry changes in permafrost after the 2002 tundra wildfire in Kougarak, Seward Peninsula, Alaska: permafrost change after a Tundra fire. *J. Geophys. Res. Earth Surf.* **121**, 1697–1715 (2016).
14. Michaelides, R. J. et al. Inference of the impact of wildfire on permafrost and active layer thickness in a discontinuous permafrost region using the remotely sensed active layer thickness (ReSALT) algorithm. *Environ. Res. Lett.* **14**, 035007 (2019).
15. Mack, M. C. et al. Carbon loss from an unprecedented Arctic tundra wildfire. *Nature* **475**, 489–492 (2011).
16. Rodríguez-Cardona, B. M. et al. Wildfires lead to decreased carbon and increased nitrogen concentrations in upland arctic streams. *Sci. Rep.* **10**, 8722 (2020).
17. Bret-Harte, M. S. et al. The response of Arctic vegetation and soils following an unusually severe tundra fire. *Phil. Trans. R. Soc. B* **368**, 20120490 (2013).
18. Taş, N. et al. Impact of fire on active layer and permafrost microbial communities and metagenomes in an upland Alaskan boreal forest. *ISME J.* **8**, 1904–1919 (2014).
19. Wardle, D. A. Long-term effects of wildfire on ecosystem properties across an island area gradient. *Science* **300**, 972–975 (2003).
20. Frost, G. V. et al. Multi-decadal patterns of vegetation succession after tundra fire on the Yukon-Kuskokwim Delta, Alaska. *Environ. Res. Lett.* **15**, 025003 (2020).
21. Heim, R. J. et al. Post-fire vegetation succession in the Siberian subarctic tundra over 45 years. *Sci. Total Environ.* **760**, 143425 (2019).
22. Racine, C. H., Johnson, L. A. & Viereck, L. A. Patterns of vegetation recovery after Tundra fires in Northwestern Alaska, U.S.A. *Arct. Alp. Res.* **19**, 461 (1987).
23. Jandt, R. R. et al. Findings of the Anaktuvuk River Fire Recovery Study, 2007–2011. (2013).
24. Klupar, I., Rocha, A. V. & Rastetter, E. B. Alleviation of nutrient co-limitation induces regime shifts in post-fire community composition and productivity in Arctic tundra. *Glob. Change Biol.* **27**, 3324–3335 (2021).
25. Wills, A. J., Cranfield, R. J., Ward, B. G. & Tunsell, V. L. Cryptogam recolonization after wildfire: leaders and laggards in assemblages? *Fire Ecol.* **14**, 65–84 (2018).
26. Hart, S. C., DeLuca, T. H., Newman, G. S., MacKenzie, M. D. & Boyle, S. I. Post-fire vegetative dynamics as drivers of microbial community structure and function in forest soils. *For. Ecol. Manag.* **220**, 166–184 (2005).
27. Holden, S. R., Rogers, B. M., Treseder, K. K. & Randerson, J. T. Fire severity influences the response of soil microbes to a boreal forest fire. *Environ. Res. Lett.* **11**, 035004 (2016).
28. Pressler, Y., Moore, J. C. & Cotrufo, M. F. Belowground community responses to fire: meta-analysis reveals contrasting responses of soil microorganisms and mesofauna. *Oikos* **128**, 309–327 (2019).
29. Wan, S., Hui, D. & Luo, Y. Fire effects on nitrogen pools and dynamics in terrestrial ecosystems: a meta-analysis. *Ecol. Appl.* **11**, 1349–1365 (2001).
30. Knicker, H. How does fire affect the nature and stability of soil organic nitrogen and carbon? A review. *Biogeochemistry* **85**, 91–118 (2007).
31. Bárcenas-Moreno, G. & Bååth, E. Bacterial and fungal growth in soil heated at different temperatures to simulate a range of fire intensities. *Soil Biol. Biochem.* **41**, 2517–2526 (2009).
32. Mabuhay, J. A., Nakagoshi, N. & Isagi, Y. Soil microbial biomass, abundance, and diversity in a Japanese red pine forest: first year after fire. *J. For. Res.* **11**, 165–173 (2006).
33. Hewitt, R. E., Bent, E., Hollingsworth, T. N., Chapin, F. S. & Taylor, D. L. Resilience of Arctic mycorrhizal fungal communities after wildfire facilitated by resprouting shrubs. *Ecoscience* **20**, 296–310 (2013).
34. Martin, A. C., Jeffers, E. S., Petrokofsky, G., Myers-Smith, I. & Macias-Fauria, M. Shrub growth and expansion in the Arctic tundra: an assessment of controlling factors using an evidence-based approach. *Environ. Res. Lett.* **12**, 085007 (2017).
35. Myers-Smith, I. H. et al. Shrub expansion in tundra ecosystems: dynamics, impacts and research priorities. *Environ. Res. Lett.* **6**, 045509 (2011).
36. Mekonnen, Z. A. et al. Arctic tundra shrubification: a review of mechanisms and impacts on ecosystem carbon balance. *Environ. Res. Lett.* **16**, 053001 (2021).
37. Güsewell, S. & Gessner, M. O. N: P ratios influence litter decomposition and colonization by fungi and bacteria in microcosms. *Funct. Ecol.* **23**, 211–219 (2009).
38. Strickland, M. S. & Rousk, J. Considering fungal:bacterial dominance in soils—methods, controls, and ecosystem implications. *Soil Biol. Biochem.* **42**, 1385–1395 (2010).
39. Malik, A. A. et al. Soil fungal:bacterial ratios are linked to altered carbon cycling. *Front. Microbiol.* **7**, 1247 (2016).
40. Mekonnen, Z. A., Riley, W. J., Randerson, J. T., Grant, R. F. & Rogers, B. M. Expansion of high-latitude deciduous forests driven by interactions between climate warming and fire. *Nat. Plants* **5**, 952–958 (2019).
41. Grant, R. F. Ecosystem CO₂ and CH₄ exchange in a mixed tundra and a fen within a hydrologically diverse Arctic landscape: 2. Modeled impacts of climate change: CO₂ and CH₄ exchange in the arctic. *J. Geophys. Res. Biogeosci.* **120**, 1388–1406 (2015).
42. Grant, R. F. et al. Mathematical modelling of Arctic Polygonal Tundra with Ecosys: 1. Microtopography determines how active layer depths respond to changes in temperature and precipitation: active layer depth in polygonal Tundra. *J. Geophys. Res. Biogeosci.* **122**, 3161–3173 (2017).
43. Mekonnen, Z. A., Riley, W. J. & Grant, R. F. 21st century tundra shrubification could enhance net carbon uptake of North America Arctic tundra under an RCP8.5 climate trajectory. *Environ. Res. Lett.* **13**, 054029 (2018).
44. Mekonnen, Z. A., Riley, W. J., Grant, R. F. & Romanovsky, V. E. Changes in precipitation and air temperature contribute comparably to permafrost degradation in a warmer climate. *Environ. Res. Lett.* **16**, 024008 (2021).
45. Mekonnen, Z. A., Riley, W. J. & Grant, R. F. Accelerated nutrient cycling and increased light competition will lead to 21st century shrub expansion in North American Arctic Tundra. *J. Geophys. Res. Biogeosci.* **123**, 1683–1701 (2018).
46. Hu, F. S. et al. Tundra burning in Alaska: linkages to climatic change and sea ice retreat. *J. Geophys. Res.* **115**, G04002 (2010).
47. Jones, B. M. et al. Fire behavior, weather, and burn severity of the 2007 Anaktuvuk River Tundra Fire, North Slope, Alaska. *Arctic Antarct., Alp. Res.* **41**, 309–316 (2009).
48. Rocha, A. V. & Shaver, G. R. Burn severity influences postfire CO₂ exchange in arctic tundra. *Ecol. Appl.* **21**, 14 (2011).
49. Bouskill, N. J., Riley, W. J., Zhu, Q., Mekonnen, Z. A. & Grant, R. F. Alaskan carbon-climate feedbacks will be weaker than inferred from short-term experiments. *Nat. Commun.* **11**, 5798 (2020).
50. Grant, R. F. Modelling changes in nitrogen cycling to sustain increases in forest productivity under elevated atmospheric CO₂ and contrasting site conditions. *Biogeosciences* **10**, 7703–7721 (2013).
51. Turetsky, M. R. et al. Recent acceleration of biomass burning and carbon losses in Alaskan forests and peatlands. *Nat. Geosci.* **4**, 27–31 (2011).
52. Gustine, R. N. From burned slopes to streams: how wildfire affects nitrogen cycling and retention in forests and fire-prone watersheds. 18.
53. Hu, F. S. et al. Arctic tundra fires: natural variability and responses to climate change. *Front. Ecol. Environ.* **13**, 369–377 (2015).
54. Bowman, D. M. J. S. et al. Vegetation fires in the anthropocene. *Nat. Rev. Earth Environ.* **1**, 500–515 (2020).
55. Davis, K. T. et al. Wildfires and climate change push low-elevation forests across a critical climate threshold for tree regeneration. *Proc. Natl. Acad. Sci. USA* **116**, 6193–6198 (2019).
56. McGuire, A. D. et al. Dependence of the evolution of carbon dynamics in the northern permafrost region on the trajectory of climate change. *Proc. Natl. Acad. Sci. USA* **115**, 3882–3887 (2018).
57. Nadelhoffer, K. J., Giblin, A. E., Shaver, G. R. & Laundre, J. A. Effects of temperature and substrate quality on element mineralization in six arctic soils. *Ecology* **72**, 242–253 (1991).
58. Monteux, S. et al. Long-term in situ permafrost thaw effects on bacterial communities and potential aerobic respiration. *ISME J.* **12**, 2129–2141 (2018).
59. Keuper, F. et al. A frozen feast: thawing permafrost increases plant-available nitrogen in subarctic peatlands. *Glob. Change Biol.* **18**, 1998–2007 (2012).
60. Keuper, F. et al. Experimentally increased nutrient availability at the permafrost thaw front selectively enhances biomass production of deep-rooting subarctic peatland species. *Glob. Change Biol.* **23**, 4257–4266 (2017).
61. Pedersen, E. P., Elberling, B. & Michelsen, A. Foraging deeply: depth-specific plant nitrogen uptake in response to climate-induced N-release and permafrost thaw in the High Arctic. *Glob. Change Biol.* **26**, 6523–6536 (2020).

62. Hewitt, R. E. et al. Mycobiont contribution to tundra plant acquisition of permafrost-derived nitrogen. *New Phytol.* **226**, 126–141 (2020).
63. Schuur, E. A. G., Crummer, K. G., Vogel, J. G. & Mack, M. C. Plant species composition and productivity following permafrost thaw and thermokarst in Alaskan Tundra. *Ecosystems* **10**, 280–292 (2007).
64. Bjorkman, A. D. et al. Plant functional trait change across a warming tundra biome. *Nature* **562**, 57–62 (2018).
65. Hudson, J. M. G. & Henry, G. H. R. Increased plant biomass in a High Arctic heath community from 1981 to 2008. *Ecology* **90**, 2657–2663 (2009).
66. Wilson, S. D. & Nilsson, C. Arctic alpine vegetation change over 20 years. *Glob. Change Biol.* **15**, 1676–1684 (2009).
67. Aerts, R. The advantages of being evergreen. *Trends Ecol. Evol.* **10**, 6 (1995).
68. Mack, M. C., Schuur, E. A. G., Bret-Harte, M. S., Shaver, G. R. & Chapin, F. S. Ecosystem carbon storage in arctic tundra reduced by long-term nutrient fertilization. *Nature* **431**, 440–443 (2004).
69. Bowman, W. D., Theodose, T. A., Schardt, J. C. & Conant, R. T. Constraints of nutrient availability on primary production in two alpine Tundra communities. *Ecology* **74**, 2085–2097 (1993).
70. Abbott, B. W. et al. Tundra wildfire triggers sustained lateral nutrient loss in Alaskan Arctic. *Glob. Change Biol.* 15507 <https://doi.org/10.1111/gcb.15507> (2021).
71. Lutsch, E. et al. Unprecedented atmospheric ammonia concentrations detected in the high arctic from the 2017 Canadian wildfires. *J. Geophys. Res. Atmos.* **124**, 8178–8202 (2019).
72. Rastetter, E. B. et al. Ecosystem recovery from disturbance is constrained by N cycle openness, vegetation-soil N distribution, form of N losses, and the balance between vegetation and soil-microbial processes. *Ecosystems* <https://doi.org/10.1007/s10021-020-00542-3> (2020).
73. Bormann, F. H. & Likens, G. E. Catastrophic disturbance and the steady state in Northern Hardwood Forests: a new look at the role of disturbance in the development of forest ecosystems suggests important implications for land-use policies. *Am. Sci.* **67**, 660–669 (1979).
74. Lovett, G. M. et al. Nutrient retention during ecosystem succession: a revised conceptual model. *Front. Ecol. Environ.* **16**, 532–538 (2018).
75. Whitman, T. et al. Soil bacterial and fungal response to wildfires in the Canadian boreal forest across a burn severity gradient. *Soil Biol. Biochem.* **138**, 107571 (2019).
76. Schimel, J. P., Kielland, K. & Chapin, F. S. Nutrient availability and uptake by Tundra plants. In: *Landscape Function and Disturbance in Arctic Tundra* (eds Reynolds, J. F. & Tenhunen, J. D.) vol. 120, pp. 203–221 (Springer Berlin Heidelberg, 1996).
77. Shaver, G. R. et al. Global change and the carbon balance of Arctic. *Ecosyst. BioSci.* **42**, 433–441 (1992).
78. Tierney, J. A., Hedin, L. O. & Wurzburger, N. Nitrogen fixation does not balance fire-induced nitrogen losses in longleaf pine savannas. *Ecology*. **100**, e02735 (2019).
79. Wong, M. Y. et al. Biological nitrogen fixation does not replace nitrogen losses after forest fires in the Southeastern Amazon. *Ecosystems* **23**, 1037–1055 (2020).
80. Norman, J. S. & Friesen, M. L. Complex N acquisition by soil diazotrophs: how the ability to release exoenzymes affects N fixation by terrestrial free-living diazotrophs. *ISME J.* **11**, 315–326 (2017).
81. Liu, X.-Y. et al. Nitrate is an important nitrogen source for Arctic tundra plants. *Proc. Natl. Acad. Sci. USA* **115**, 3398–3403 (2018).
82. Ball, P. N., MacKenzie, M. D., DeLuca, T. H. & Holben, W. E. Wildfire and charcoal enhance nitrification and ammonium-oxidizing bacterial abundance in dry montane forest soils. *J. Environ. Qual.* **39**, 11 (2010).
83. Kurth, V. J., Hart, S. C., Ross, C. S., Kaye, J. P. & Fulé, P. Z. Stand-replacing wildfires increase nitrification for decades in southwestern ponderosa pine forests. *Oecologia* **175**, 395–407 (2014).
84. Stephan, K., Kavanagh, K. L. & Koyama, A. Comparing the influence of wildfire and prescribed burns on watershed nitrogen biogeochemistry using 15N natural abundance in terrestrial and aquatic ecosystem components. *PLoS ONE* **10**, e0119560 (2015).
85. Jiang, Y. et al. Modeling long-term changes in tundra carbon balance following wildfire, climate change, and potential nutrient addition. *Ecol. Appl.* **27**, 105–117 (2017).
86. Rustad, L. et al. A meta-analysis of the response of soil respiration, net nitrogen mineralization, and aboveground plant growth to experimental ecosystem warming. *Oecologia* **126**, 543–562 (2001).
87. Xue, K. et al. Tundra soil carbon is vulnerable to rapid microbial decomposition under climate warming. *Nat. Clim. Change* **6**, 595–600 (2016).
88. Schimel, J. P. & Bennett, J. Nitrogen mineralization: challenges of a changing paradigm. *Ecology* **85**, 591–602 (2004).
89. Sorensen, P. O. et al. The snowmelt niche differentiates three microbial life strategies that influence soil nitrogen availability during and after winter. *Front. Microbiol.* **11**, 871 (2020).
90. Bilbrough, C. J., Welker, J. M. & Bowman, W. D. Early spring nitrogen uptake by snow-covered plants: a comparison of Arctic and Alpine plant function under the snowpack. *Arctic, Antarct. Alp. Res.* **32**, 404–411 (2000).
91. Kwon, M. J. et al. Drainage enhances modern soil carbon contribution but reduces old soil carbon contribution to ecosystem respiration in tundra ecosystems. *Glob. Change Biol.* **25**, 1315–1325 (2019).
92. Chipman, M. L. et al. Spatiotemporal patterns of tundra fires: late-quaternary charcoal records from Alaska. *Biogeosciences* **12**, 4017–4027 (2015).
93. Fernández-García, V. et al. Fire regimes shape diversity and traits of vegetation under different climatic conditions. *Sci. Tot. Environ.* **716**, 137137 (2020).
94. Dove, N. C., Klingeman, D. M., Carrell, A. A., Cregger, M. A. & Schadt, C. W. Fire alters plant microbiome assembly patterns: integrating the plant and soil microbial response to disturbance. *New Phytol.* **230**, 2433–2446 (2021).
95. Grant, R. F. Simulation of ecological controls on nitrification. *Soil Biol. Biochem.* **26**, 305–315 (1994).
96. Grant, R. F. Simulation of methanotrophy in the mathematical model ecosys. *Soil Biol. Biochem.* **31**, 287–297 (1999).
97. Grant, R. F. & Rochette, P. Soil microbial respiration at different water potentials and temperatures: theory and mathematical modeling. *Soil Sci. Soc. Am. J.* **58**, 10 (1994).
98. Grant, R. F., Juma, N. G. & McGill, W. B. Simulation of carbon and nitrogen transformations in soil: mineralization. *Soil Biol. Biochem.* **25**, 1317–1329 (1993).
99. Schmidt, M. W. I. et al. Persistence of soil organic matter as an ecosystem property. *Nature* **478**, 49–56 (2011).
100. Mougnot, C. et al. Elemental stoichiometry of fungi and bacteria strains from grassland leaf litter. *Soil Biol. Biochem.* **76**, 278–285 (2014).
101. Liu, S. et al. The Unified North American Soil Map and its implication on the soil organic carbon stock in North America. *Biogeosciences* **10**, 2915–2930 (2013).
102. Grant, R. F., Mekonnen, Z. & Riley, W. J. Modeling climate change impacts on an arctic polygonal tundra: 1. rates of permafrost thaw depend on changes in vegetation and drainage. *JGR Biogeosciences*. **124**, 1308–1322 (2019).
103. Meinshausen, M. et al. The RCP greenhouse gas concentrations and their extensions from 1765 to 2300. *Clim. Change* **109**, 213–241 (2011).
104. Dentener, F. et al. Nitrogen and sulfur deposition on regional and global scales: a multimodel evaluation: multimodel global deposition. *Glob. Biogeochem. Cycles*. **20**, GB4003 (2006).
105. Kalnay, E. et al. The NCEP/ NCAR 40-year reanalysis project. *Bull. Am. Meteorol. Soc.* **77**, 437–471 (1996).
106. Ruddell, B. L. & Kumar, P. Ecohydrologic process networks: 1. Identification: ecohydrologic process networks, 1. *Water Resour. Res.* **45**, W03419 (2009).

Acknowledgements

This research was supported by the Director, Office of Science, Office of Biological and Environmental Research of the U.S. Department of Energy under contract DE-AC02-05CH11231 to Lawrence Berkeley National Laboratory as part of the Next-Generation Ecosystem Experiments in the Arctic (NGEE Arctic) project.

Author contributions

N.J.B. and W.J.R. designed the scope of the work, and N.B. ran the experimental simulations. Z.M. helped with model set-up. Z.M. and R.G. helped with model benchmarking. Q.Z. assisted with the causality analysis. N.J.B. wrote the manuscript with input from all co-authors.

Competing interests

The authors declare no competing interests.

Additional information

Supplementary information The online version contains supplementary material available at <https://doi.org/10.1038/s43247-022-00356-2>.

Correspondence and requests for materials should be addressed to Nicholas J. Bouskill.

Peer review information *Communications Earth & Environment* thanks Nicholas Dove and the other, anonymous, reviewer(s) for their contribution to the peer review of this work. Primary Handling Editors: Clare Davis. Peer reviewer reports are available.

Reprints and permission information is available at <http://www.nature.com/reprints>

Publisher's note Springer Nature remains neutral with regard to jurisdictional claims in published maps and institutional affiliations.



Open Access This article is licensed under a Creative Commons Attribution 4.0 International License, which permits use, sharing, adaptation, distribution and reproduction in any medium or format, as long as you give appropriate credit to the original author(s) and the source, provide a link to the Creative Commons license, and indicate if changes were made. The images or other third party material in this article are included in the article's Creative Commons license, unless indicated otherwise in a credit line to the material. If material is not included in the article's Creative Commons license and your intended use is not permitted by statutory regulation or exceeds the permitted use, you will need to obtain permission directly from the copyright holder. To view a copy of this license, visit <http://creativecommons.org/licenses/by/4.0/>.

© The Author(s) 2022